applied sciences

MDPI

*Article*

# Investigation of Adsorption and Young's Modulus of Epoxy Resin–Sand Interfaces Using Molecular Dynamics Simulation

**Dejian Shen [1,*], Xueran Pi [1], Lili Cai [2], Xin Wang [1], Chunying Wu [2] and Ruixin Liu [1]**

[1] College of Civil and Transportation Engineering, Hohai University, Nanjing 210098, China; xueranpi@163.com (X.P.); wangstar@hhu.edu.cn (X.W.); liuruixin525@163.com (R.L.)
[2] Nanjing Ningtong Intelligent Transportation Technology Research Institute Co., Ltd., Nanjing 211135, China; cll@jsti.com (L.C.); wcytrans@126.com (C.W.)
* Correspondence: hohaicivil@gmail.com

**Abstract:** Epoxy resins exhibit outstanding curability, durability, and environmental compatibility, rendering them extensively utilized in the realm of engineering curing. Nevertheless, the current curing mechanism of epoxy-based resins in cohesion with sand remains inadequately elucidated, significantly impeding their applicability within the domain of soil curing. This study employed molecular dynamics simulations to investigate the adsorption behavior of three distinct types of epoxy resins on the sand surface: diglycidyl ether of bisphenol-A epoxy resin (DGEBA), diglycidyl ether 4,4′-dihydroxy diphenyl sulfone (DGEDDS), and aliphatic epoxidation of olefin resin (AEOR). The objective was to gain insights into the interactions between the sand surface and the epoxy resin polymers. The results demonstrated that DGEDDS formed a higher number of hydrogen bonds on the sand surface, leading to stronger intermolecular interactions compared to the other two resins. Furthermore, the mechanical properties of the adsorbed models of the three epoxy resins with sand were found to be relatively similar. This similarity can be attributed to their comparable chemical structures. Finally, analysis of the radius of gyration for the adsorbed epoxy resins revealed that AEOR exhibited a rigid structure due to strong molecular interactions, while DGEDDS displayed a flexible structure owing to weaker interactions.

**Keywords:** epoxy resins; sand; molecular dynamics simulation; adsorption



**Citation:** Shen, D.; Pi, X.; Cai, L.; Wang, X.; Wu, C.; Liu, R. Investigation of Adsorption and Young's Modulus of Epoxy Resin–Sand Interfaces Using Molecular Dynamics Simulation. *Appl. Sci.* **2024**, *14*, 10383. https://doi.org/10.3390/app142210383

Academic Editor: Francesco Stellato

Received: 26 September 2024
Revised: 24 October 2024
Accepted: 8 November 2024
Published: 12 November 2024



## 1. Introduction

Among various types of natural soils, sand stands as the predominant resource, with an annual consumption of approximately five billion tons [1]. Its widespread utilization encompasses crucial sectors such as road engineering [2] and foundation construction [3], among others. Nevertheless, owing to its inherently loose structure, extensive interparticle voids, and limited cohesive properties, sand is regarded as a problematic soil medium that cannot be employed directly in engineering construction projects. In the absence of proper mitigation measures, a high proportion of loose sandy subsoil in the foundation can give rise to insufficient bearing capacity, consequently triggering a cascade of challenges including building inclination, roadbed settlement, and slope instability [4,5]. It is imperative to implement appropriate measures for the treatment of sand to mitigate these issues effectively. The prevalent techniques employed for the stabilization of sand can be broadly classified into mechanical stabilization and chemical curing [6]. Mechanical stabilization entails the employment of machinery, such as road rollers and vibratory compactors, to compact the sand and enhance its density. On the other hand, chemical curing involves the introduction of external agents that trigger physical or chemical reactions, thereby imparting a certain level of strength to the sand. Mechanical stabilization exhibits drawbacks including difficulties in equipment transportation, high noise levels, significant energy consumption, and extended construction periods. Compared with mechanical stabilization,

utilizing curing agents for soil stabilization presents several benefits including shorter construction periods, lower consumption, and minimal environmental impact. The primary curing agents employed for sand stabilization encompass lime [7–9], bio-enzymes [10–12], and polymers [13–15]. The application of lime as a curing agent in engineering projects is often hindered by challenges including high consumption rates, elevated transportation costs, and relatively low early-age strength [16]. The utilization of bio-enzymes as curing agents poses challenges, such as the instability of their effects and the significant influence of environmental factors on the solidification efficacy [17,18]. Polymer-based curing agents present notable advantages, such as minimal dosing requirement, convenient transportation, simplified application process, and steadfast efficacy [19,20].

Liu et al. [21] conducted a study on the reinforcement of sand using different types of short fibers and organic polymer, revealing that the incorporation of composite materials exerts a substantial influence on the strength and modulus. Yuan et al. [22] developed a novel sand-fixing curing agent and substantiated its outstanding mechanical properties through rigorous experimental validation. Previous studies have primarily focused on non-epoxy-based polymers, with comparatively limited investigations conducted on polymers incorporating epoxy functional groups. The study conducted by Anastassiou et al. [23] reveals that the introduction of oxygen atoms into polymer molecules exhibits a substantial enhancement in their adsorption energy. Meanwhile, epoxy polymers are characterized by the presence of two or more epoxy groups, and they find extensive application as curing agents for polymeric materials owing to their outstanding cohesive properties, corrosion resistance, and rheological characteristics [24,25]. Notable examples of epoxy polymers encompass the diglycidyl ether of bisphenol-A epoxy resin (DGEBA), the diglycidyl ether of 4,4′-dihydroxy diphenyl sulfone (DGEDDS), and aliphatic epoxidation of olefin resin (AEOR), among others. In light of the foregoing, it is evident that the existing body of research predominantly revolves around non-epoxy-based polymers, with a relative scarcity of investigations specifically targeting the curing aspects of epoxy polymers. Consequently, the current state of knowledge fails to offer comprehensive insights into predicting the curing efficacy of epoxy polymers, primarily attributed to the ongoing ambiguity surrounding the underlying mechanisms governing their curing behavior. The study on the solidification mechanism of epoxy polymers in sand endeavors to unveil the fundamental principles governing the solidification process, to facilitate the widespread adoption of soil solidification techniques utilizing epoxy polymers, and to furnish a robust theoretical foundation and technical guidance for practical implementation.

Molecular dynamics simulation methods have established themselves as valuable research approaches for studying the formation mechanisms of materials at the nanoscale [26–29]. The macroscopic properties of epoxy copolymer curing agents are intrinsically governed by their nanoscale. Molecular dynamics simulation enables the precise quantification of intermolecular interactions among diverse materials, facilitating a comprehensive molecular-level comprehension of the intricate mechanisms governing their interplay [30–32]. Huang et al. [33] conduct a comprehensive molecular dynamics investigation on the adsorption and modification mechanisms of polymer curing agents, and the study crucially demonstrates the paramount importance of the functional groups of the polymers in the adsorption process. Ma et al. [25] employ the molecular dynamics method to investigate the thermomechanical properties of molecular structures influenced by epoxy resin curing agents, and the findings reveal a direct relationship between the length of the molecular chain and the polarity of functional groups, indicating that longer chains and smaller polarity of functional groups diminish the thermomechanical properties of the curing process. Nevertheless, a comprehensive investigation utilizing molecular dynamics methods to delve into the nanoscale mechanisms governing the curing of epoxy polymers in sand remains noticeably absent in existing research. Moreover, the precise mechanisms governing the interaction between epoxy polymer curing agents and sand remain uncertain. Therefore, there is a compelling imperative to employ a molecular dy-

namics simulation to decipher the intricate mechanisms underlying the curing process of epoxy polymers in sand.

The physical adsorption process stands as a pivotal stage during the material curing process, dictating the specific mode of bonding between the curing agent and the surface of the sand particles [34]. Lyu et al. [35] conduct a study on the adsorption mechanism of a branched quaternary ammonium salt gemini surfactant at the water–quartz–water interface, unveiling the underlying microscopic adsorption mechanism of the surfactant on the quartz surface. Quezada et al. [36] conduct a molecular dynamics study to examine the adsorption behavior of six polymers on quartz surfaces in different salinities. The findings reveal that the favorable or unfavorable adsorption of the polymers is predominantly governed by their electrical charge, highlighting the influential role of salinity in mediating this process. Cheng et al. [37] conduct a study on the adsorption mechanisms of 3-dodecyloxypropylamine, 3-tetradecyloxypropylamine, and dodecylamine on the quartz (1 0 1) surface, employing a combination of micro-flotation experiments and an ab initio molecular dynamics simulation. The aforementioned studies on the adsorption mechanisms of polymers on quartz, based on molecular simulation, have yielded some preliminary results. Nevertheless, it is worth noting that the polymers investigated in these studies do not feature epoxy groups, making their research systems distinct from the epoxy polymer–soil systems employed in the solidification of sand. Consequently, the obtained findings are not directly transferrable to the solidification of epoxy polymers in sand. Therefore, it is imperative to undertake pertinent investigations regarding the adsorption of epoxy polymers on the surface of sand.

The geotechnical properties of soil have a direct impact on its deformation characteristics, while soil deformation is closely correlated with the analysis and design of the foundation bearing capacity. Therefore, investigating the bulk modulus, shear modulus, Young's modulus, and Poisson's ratio of stabilized sand represents essential performance parameters for evaluating the efficiency of sand consolidation. Zhang et al. [38] conduct measurements and analyses on the microcosmic pattern, mechanical properties, and specific surface area of fiber-reinforced quartz composites. The findings reveal that the modified composites exhibit outstanding mechanical properties and moisture resistance. Yuan et al. [22] propose a novel sand-fixing curing agent, a nanosilica/polymer composite material, and conduct a microscale investigation on the mechanical properties and hydration mechanism of the resultant material. The findings demonstrate that the nanosilica/polymer composite material effectively agglomerates the sand particles and enhances the overall strength of the system. Zhang et al. [39] implement a geopolymer based on ground granulated blast-furnace slag and fly ash to reinforce sand. The composites are investigated by adjusting the type and ratio of the exciter, water–cement ratio, curing conditions, and slag–fly ash ratio. The results unequivocally demonstrate the remarkable efficacy of the geopolymer, formulated with ground granulated blast-furnace slag and fly ash, in substantially improving the mechanical property of the sand. Despite extensive studies on the reinforcement of sand with polymers at the nanoscale by numerous scholars, there has been limited research on the mechanical behavior of epoxy polymers when they solidify sand using molecular dynamics simulation. Therefore, it is necessary to investigate the mechanical properties of epoxy polymers adsorbed onto sand.

Despite the extensive application of epoxy polymers in the solidification of sand, a thorough investigation of the nanoscale mechanisms involved in the epoxy polymerization process for sand solidification is still lacking. This study utilized molecular dynamics simulation to construct molecular models of three different systems, DGEBA, DGEDDS, and AEOR, adsorbed onto sand. The aim was to investigate their adsorption behavior and mechanical properties, including volume modulus and shear modulus. Firstly, molecular models of epoxy polymers and sand crystals were established. Subsequently, molecular dynamics simulation was employed to study the adsorption process of the three epoxy polymers on sand. Finally, various parameters such as the count of hydrogen bonds, adsorption energies, and mechanical properties were computed for each system. By

utilizing molecular dynamics simulation to investigate the molecular behavior of epoxy polymer curing agents on sand, this study offered a comprehensive understanding of the adsorption mechanisms at the atomic scale and conducted an in-depth analysis of the relevant mechanical property parameters of the composite systems.

## 2. Simulation Methods

### *2.1. Molecular Model of Epoxy Resins*

DGEBA, DGEDDS, and AEOR were utilized as material models to investigate mechanism of sand cured by epoxy resin. DGEBA is a kind of polymer containing bisphenol A and epoxy group functional groups, forming a three-dimensional network structure with high properties through the reaction between them. DGEDDS with bisphenol S and epoxy group functional groups was also selected in the study. In addition, EOR was also selected as the third polymer to validate that the inclusion of oxygen atoms can improve the adsorption capacity. Among the three types of epoxy resin, DGEBA and the DGEDDS belong to glycerol ether epoxy resin; however, AEOR belongs to linear aliphatic epoxy compounds. The epoxy group is the characteristic group of epoxy resin, and its content is an important indicator to evaluate the nature of a substance. There are two main parameters to describe the content of the epoxy group, the namely epoxy equivalent and epoxy value. The epoxy equivalent refers to the quality of 1mol of epoxy resin; the epoxy value refers to the amount of epoxy substance contained in 100g of resin. The latter is often used for the measurement of curing agents and the expression of the amount, and the epoxy value was adopted in this study. To ensure that each resin had a similar molecular weight, the simulation was controlled to have about 50 carbon atoms [33]. In the practical application process, it is also necessary to control the ratio relationship between the soil and curing agent to calculate the dosage, and the specific parameters are shown in Table 1.

**Table 1.** Parameters for three types of epoxy resins.

| Types of Epoxy Resins | Chemical Formula | Molecular Weight ($g \cdot mol^{-1}$) | Epoxy Value (mol) | References |
|---|---|---|---|---|
| DGEBA | $C_{57}H_{64}O_{10}$ | 904 | 0.222 | [40] |
| DGEDDS | $C_{48}H_{46}O_{16}S_3$ | 870 | 0.230 | [41] |
| AEOR | $C_{56}H_{86}O_{14}$ | 983 | 1.424 | [42] |

Among the epoxy resins, DGEBA is known as the universal epoxy resin, and its yield is the largest, because its raw material is easy to obtain and its cost is the lowest. In this study, the polymerization degree n of DGEBA was set to be 2. The structural formula and the corresponding molecular model are shown in Figures 1a and 1b, respectively.

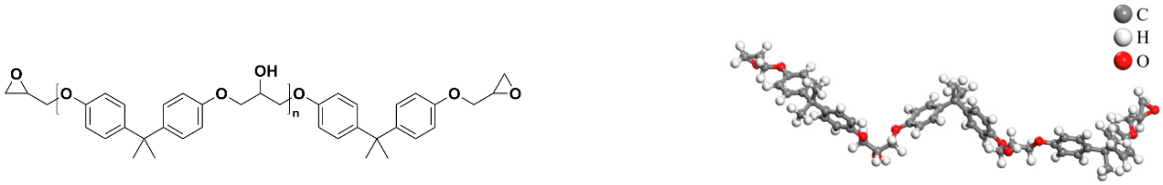


(**a**) (**b**)

**Figure 1.** Structural formula and molecular model of DGEBA. (**a**) Structural formula; (**b**) molecular model.

DGEDDS has excellent heat resistance due to it containing sulfur. In this study, the polymerization degree n of DGEDDS was set to be 2, and its structural formula is shown in Figure 2a. Due to the molecular structural formula containing two hydroxyl groups and one sulfone group, DGEBA is more acidic compared to both DGEBA and AEOR. The structural formula is shown in Figure 2b.

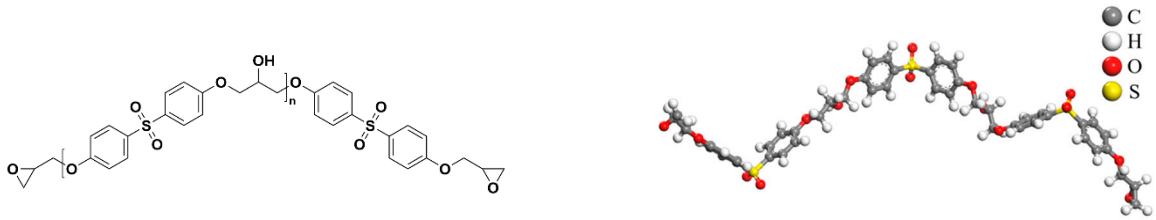


(**a**) (**b**)

**Figure 2.** Structural formula and molecular model of DGEDDS. (**a**) Structural formula; (**b**) molecular model.

AEOR is prepared by oxidizing the double bonds of aliphatic epoxy olefin [43]. Based on its structural formula, it can be observed that AEOR predominantly comprises carbon chains and possesses multiple epoxy groups within its molecular structure. In this study, the polymerization degree n of AEOR was set to be 7. The structural formula and the corresponding molecular model are shown in Figures 3a and 3b, respectively.

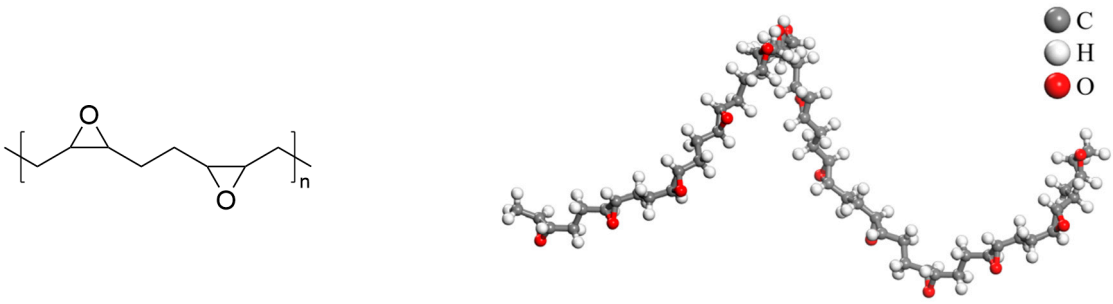


(**a**) (**b**)

**Figure 3.** Structural formula and molecular model of AEOR. (**a**) Structural formula; (**b**) molecular model.

Through Forcite in the software of Materials Studio (version 1.9.4), the molecular model of each compound was optimized to find the lowest energy state of the structure, so as to ensure the stable existence of each compound and cure the soil.

### *2.2. Molecular Model of Sand*

Sand is predominantly composed of minerals such as quartz, mica and feldspar, with quartz constituting the highest proportion. And quartz is mainly composed of silica. Consequently, silica was selected as the sand model for this study, and its chemical formula is $SiO_2$ [44]. In the crystal structure of silica, silicon atoms are situated at the center of a silicon–oxygen tetrahedron, while oxygen atoms occupy the four tetrahedral vertices. Silicon atoms and oxygen atoms are covalently bonded through sigma ($\sigma$) bonds, thereby establishing the structural framework of the silicon–oxygen tetrahedron. The simulated silica crystal is hydroxylated due to the instability of the exposed oxygen atoms on the surface and the charge imbalance of the system [45]. The layered crystal structure of sand is shown in Figure 4.

The supercell was constructed on the model of a single-unit silica cell, its (0 0 1) crystal surface was cleaved, and the vacuum slab was built so that the lattice length was 35.40 Å. Periodic boundary conditions were used to keep the density constant in the calculation. Finally, a lattice with a total atomic number of 1980 was obtained. And its specific lattice size is shown in Figure 5.

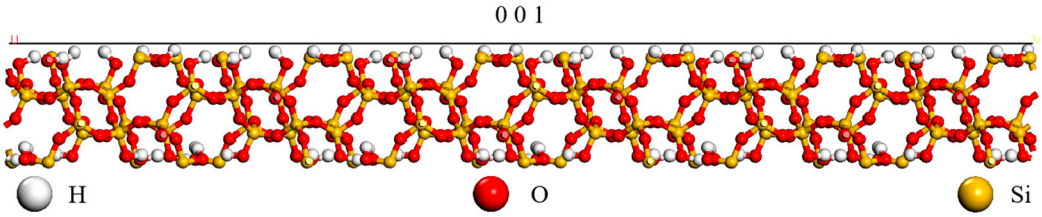


**Figure 4.** Layered crystal structure of sand (0 0 1).

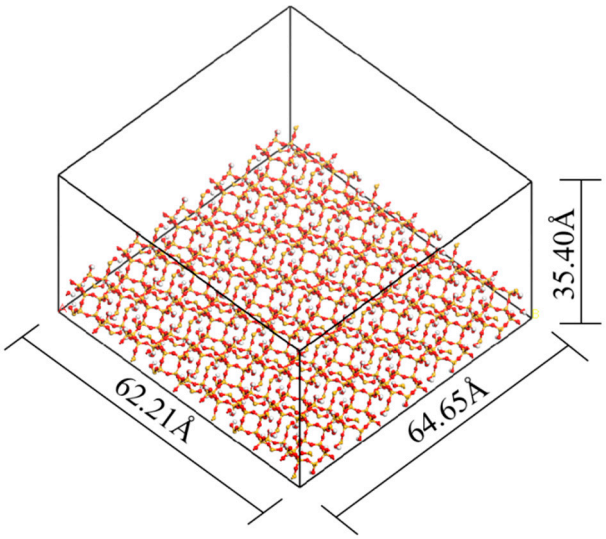


**Figure 5.** Molecular model of sand crystal structure.

Based on the model constructed above, three combination models between three resins and sand crystal structure could be obtained, as shown in Figure 6. The interface model between sand and DGEBA is designated as DGEBA–Sand, while the interface model between sand and DGEDDS is referred to as DGEDDS–Sand. Similarly, the interface model between sand and AEOR is denoted as AEOR–Sand.

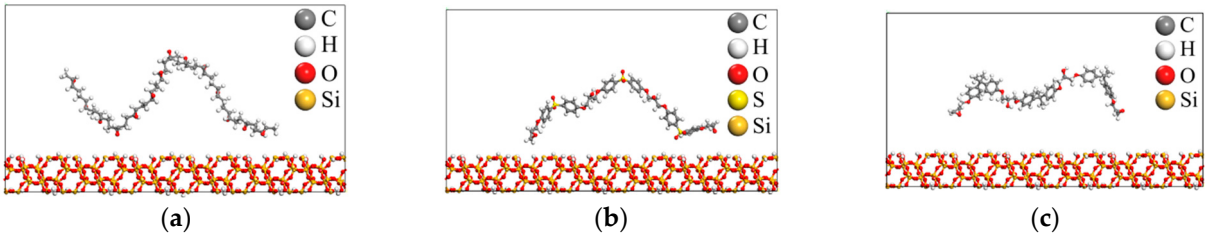


**Figure 6.** Interface model of epoxy resin and sand: (**a**) DGEBA–Sand; (**b**) DGEDDS–Sand; (**c**) AEOR–Sand.

### *2.3. Molecular Simulation*

Molecular dynamics simulation is a computational methodology rooted in classical mechanics, specifically utilizing molecular force fields to numerically integrate the equations of motion for a molecular system. This approach enables the investigation of the structural organization and properties of said molecular system through computer-simulated trajectories and statistical analyses [46]. In this study, molecular models were constructed at the atomic level using Materials Studio [47] (a software platform designed for conducting material simulation, computational analysis, and design). Subsequently, the choice of the COMPASS force field was determined through a comprehensive compositional analysis. The COMPASS (condensed-phase optimized molecular potentials for atomistic simulation studies) force field is a rigorously developed potential energy model

that combines ab initio calculation and empirical data parametrization [48]. Primarily utilized in atomistic simulation studies, this force field allows for the precise optimization of molecular potentials in condensed phases. It enables accurate predictions of the structural organization, conformational dynamics, vibrational properties, and thermodynamic behaviors of both isolated and condensed molecules. Empirical evidence from numerous studies conclusively supports the use of this force field in investigations encompassing both organic and inorganic systems [46,47]. The NVT ensemble (canonical ensemble) was used, and the system initial temperature was set at 298K. Temperature was controlled by using the Nose–Hoover method, and the simulation time was 10ns. The attainment of an equilibrium state was observed when the total energy of the system converges. Subsequent to this, computational assessments were performed to determine the adsorption energy of the resin and soil, the interface hydrogen bonds after the adsorption, and the mechanical characteristics. To avoid trapping in a single potential well, a minimum distance of 5Å was maintained between the resin and the silica surface during the initial stages of the simulation. When analyzing the adsorption energy and the hydrogen bonds of all configurations, default values were employed for the maximum hydrogen acceptor distance and minimum donor–hydrogen–acceptor angle, which were set at 2.5 Å and 90°, respectively.

### *2.4. Epoxy Resin–Sand Surface Interactions*

Apart from physical interactions, molecular systems may also involve weak chemical interactions induced by electron transfer [49]. One prominent example of such weak chemical interaction is hydrogen bonding [50]. Hydrogen bonding, being an exceptional type of intermolecular force, exerts a pivotal role in surface adsorption phenomena. In this study, the combination models were examined using Materials Studio to calculate the hydrogen bonds. The hydrogen bonds in the resin and sand models were also analyzed. Subsequently, the number of the interface hydrogen bonds after the adsorption was determined according to Equation (1):

$$N_{surface} = N_{total} - N_{resin} - N_{sand} \quad (1)$$

where $N_{surface}$ denotes the count of the interface hydrogen bonds after the adsorption, $N_{total}$ signifies the total number of hydrogen bonds encompassing all atoms within the comprehensive system, $N_{resin}$ corresponds to the intrinsic count of hydrogen bonds associated with the resin, and $N_{sand}$ represents the inherent count of hydrogen bonds pertaining to the sand.

To eliminate the influence of molecular weight differences and better highlight the contribution of hydrogen bonding in adsorption, the number of hydrogen bonds per unit molecular weight ($N_{unit}$) was introduced to compare the adsorption performance of the three resins on the sand surface. Equation (2) was employed for calculation purposes [33]:

$$N_{unit} = N_{surface} / M_{resin} \quad (2)$$

where $N_{surface}$ denotes the count of the interface hydrogen bonds generated at the interfacial region, while $M_{resin}$ represents the molecular weight of the epoxy resin.

The adsorption energy represents the capacity of a material to adhere to other substances, and its magnitude plays a crucial role in determining the speed and efficiency of material adsorption. Therefore, understanding the adsorption energy is vital for investigating the curing process of sand with curing agents [34]. Under vacuum conditions, the adsorption energy of a material can be calculated using Equation (3) [51]:

$$E_{ads} = E_{total} - E_{polymer} - E_{quartz} \quad (3)$$

where $E_{total}$ corresponds to the configurational energy of the overall system comprising all constituent atoms in kcal $\cdot$ mol$^{-1}$, $E_{polymer}$ relates to the configurational energy specific to the polymer in kcal $\cdot$ mol$^{-1}$, $E_{quartz}$ represents the configurational energy associated with the sand, specifically quartz in kcal $\cdot$ mol$^{-1}$, while $E_{ads}$ signifies the adsorption energy

at the interface of adsorption in kcal · mol$^{-1}$. $E_{ads}$ governs the intermolecular interaction energy necessary for the polymer to disrupt the surface of the sand, concurrently serving as a measure of the adhesive strength at the interface.

The radius of gyration is a critical parameter in molecular dynamics simulations, providing valuable insights into both the structural arrangement and dynamic behavior of epoxy resin–sand systems. This property can be leveraged to predict the mechanical properties of these composites, optimize their design for enhanced performance, and gain a deeper understanding of the interfacial interactions occurring at the epoxy resin–sand surface. The radius of gyration, which quantifies a molecule's spatial extension, can be calculated as follows:

$$Rg^2 = (\sum_i \|r_i\|^2 m_i) / \sum_i m_i \quad (4)$$

where $m_i$ is the mass of atom $i$, and $r_i$ is the distance of the atom $i$ in the molecule from their common center of mass.

## 3. Results and Discussion

### 3.1. Hydrogen Bond Analysis

The specific outcomes are meticulously documented and presented in Table 2. The differing molecular structures of various epoxy resin types resulted in variations in their hydrogen bonding capabilities. The hydroxyl groups present on the sand surface also influenced hydrogen bond formation. These discrepancies led to distinct migration, diffusion, and degradation behaviors of different epoxy resin types within the sand, ultimately affecting their performance in practical applications. DGEBA did not form hydrogen bonds with sand, indicating that the adsorption between DGEBA and sand was primarily driven by non-polar interactions such as van der Waals forces and electrostatic interactions. This suggests that the adsorption strength between DGEBA and sand was relatively weak, potentially leading to easier detachment from the sand surface. DGEDDS formed eight hydrogen bonds with sand, signifying strong polar interactions between the resin and sand. The formation of hydrogen bonds significantly enhanced the adsorption strength between DGEDDS and sand, resulting in more stable adsorption on the sand surface. AEOR only formed one hydrogen bond with sand, suggesting weaker polar interactions compared to DGEDDS. However, the interaction still existed, making the adsorption strength of AEOR slightly stronger than that of DGEBA, but significantly weaker than that of DGEDDS.

**Table 2.** Number of interface hydrogen bonds and number of hydrogen bonds per unit molecular weight for the three models.

| Adsorption System Types | $N_{total}$ | $N_{resin}$ | $N_{sand}$ | $N_{surface}$ | $N_{unit}$ |
|---|---|---|---|---|---|
| DGEBA-Sand | 174 | 0 | 174 | 0 | 0 |
| DGEDDS-Sand | 192 | 2 | 182 | 8 | $9.188 \times 10^{-3}$ |
| AEOR-Sand | 151 | 0 | 150 | 1 | $1.017 \times 10^{-3}$ |

The interface hydrogen bond count per unit molecular weight at the interface was found to be 0 for DGEBA, $9.188 \times 10^{-3}$ for DGEDDS, and $1.017 \times 10^{-3}$ for AEOR. By combining an analysis of the number of hydrogen bonds and the number of hydrogen bonds per unit molecular weight, the following conclusions were drawn: The molecular structure of DGEDDS enabled it to form a large number of hydrogen bonds with sand. Moreover, these hydrogen bonds maintained a high density even on a per-unit-molecular-weight basis. This explained the strong adsorption capacity of DGEDDS. While AEOR exhibited a certain degree of hydrogen bonding with sand, its strength and quantity were lower than those of DGEDDS. The adsorption between DGEBA and sand was primarily driven by non-polar forces. These results highlighted the significant contribution of hydrogen bonding to the adsorption of epoxy resins on sand, particularly in the case of DGEDDS.

### 3.2. Adsorption Energy Analysis

The adsorption energies at the interfaces ($E_{ads}$) of DGEBA, the DGEDDS, and the AEOR were determined to be −56.97, −76.54, and −74.70 kcal · mol$^{-1}$, respectively, as shown in Figure 7. A higher adsorption energy indicated stronger adsorption strength. The adsorption energy data aligned with those of the previous analysis based on the number of hydrogen bonds and the number of hydrogen bonds per unit molecular weight. DGEDDS exhibited the strongest adsorption strength. While AEOR formed fewer hydrogen bonds, its adsorption energy remained relatively high, indicating that hydrogen bonding was still the primary force governing its interaction with sand. DGEBA, due to its lack of hydrogen bond formation, exhibited the lowest adsorption energy and weakest adsorption strength.

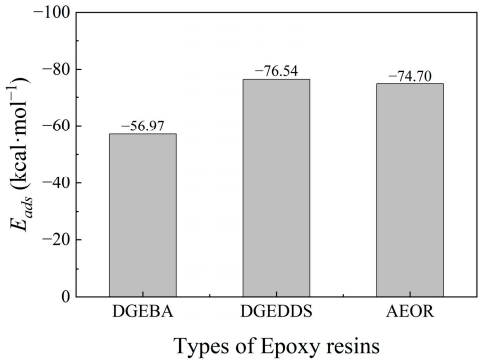


**Figure 7.** The adsorption energies of the three epoxy resins on the sand surface.

### 3.3. Mechanical Property Analysis

This study employed a stress fluctuation method to calculate the mechanical properties of the system. Under a constant temperature, T, the relationship between the elastic stiffness coefficient ($C_{ijkl}$) and the stress ($\sigma_{ij}$, N · m$^{-2}$) and strain ($\varepsilon_{kl}$) can be obtained using Equation (5) [52]:

$$C_{ijkl} = \left.\frac{\partial \sigma_{ij}}{\partial \sigma_{kl}}\right|_{T,\varepsilon_{kl}} = \frac{1}{V_0}\left.\frac{\partial^2 A}{\partial \varepsilon_{ij}\partial \varepsilon_{kl}}\right|_{T,\varepsilon_{ij},\varepsilon_{kl}} \quad (5)$$

where $V_0$ represents the initial volume of the simulation unit in its undeformed state, m$^3$, and $A$ denotes the Helmholtz free energy in J. By utilizing Equations (6) to (9), the computation of two distinct coefficients, namely the bulk modulus ($K$, GPa) and the shear modulus ($G$, GPa), enables the characterization of the elastic properties of isotropic materials.

$$G_V = [C_{11} + C_{22} + C_{33} + 2(C_{44} + C_{55} + C_{66}) - (C_{12} + C_{13} + C_{23})]/15 \quad (6)$$

$$G_R = 15/[4(S_{11} + S_{22} + S_{33} - S_{12} - S_{13} - S_{23}) + 3(S_{44} + S_{55} + S_{66})] \quad (7)$$

$$K_V = [C_{11} + C_{33} + 2(C_{21} + C_{13} + C_{23})]/9 \quad (8)$$

$$K_R = [S_{11} + S_{22} + S_{33} + 2(S_{12} + S_{13} + S_{23})]^{-1} \quad (9)$$

where the subscripts $R$ and $V$ refer to the Reuss and Voigt average values, respectively. $S_{ij}$ represents the components of the elastic compliance matrix derived from the inverse of the elastic stiffness matrix. Hill represents the actual values of the bulk and shear moduli, which typically fall within the range of the Reuss and Voigt values. This approximation is commonly known as the Voigt–Reuss–Hill (VRH) approximation. The bulk modulus and shear modulus of the system can be determined using Equations (10) and (11) [53]:

$$K_{VRH} = (K_V + K_R)/2 \quad (10)$$

$$G_{VRH} = (G_V + G_R)/2 \quad (11)$$

Utilizing the average values from the aforementioned two methods, the calculation of Young's modulus ($E$, GPa) and Poisson's ratio ($v$) can be achieved through Equations (12) and (13):

$$E = 9G_{VRH}/(3 + G_{VRH}/K_{VRH}) \quad (12)$$

$$v = (3 - 2G_{VRH}/K_{VRH})/(6 + 2G_{VRH}/K_{VRH}) \quad (13)$$

The mechanical properties of the three epoxy resins did not differ significantly, as shown in Table 3. After adsorption with sand, DGEBA exhibited a slightly higher shear modulus and Young's modulus compared to the other two epoxy resins, indicating a stronger resistance to shear and tensile deformation. Furthermore, its Poisson's ratio was slightly higher in the XY direction than those of the other epoxy resins, suggesting increased susceptibility to transverse deformation in that direction.

**Table 3.** The computed mechanical properties of the three interface models.

| Interface Models | Value of Bulk Modulus (GPa) | Value of Shear Modulus (GPa) | Value of Young's Modulus (GPa) | Value of Poisson's Ratio | |
|---|---|---|---|---|---|
| DGEBA–Sand | 29.5767 (Reuss)<br>29.5878 (Voigt)<br>29.5823 (Hill) | 17.7002 (Reuss)<br>18.6745 (Voigt)<br>18.1874 (Hill) | 45.8205 (X)<br>45.6388 (Y)<br>51.5474 (Z) | 0.2803 (XY)<br>0.1942 (XZ)<br>0.2792 (YX) | 0.1965 (YZ)<br>0.2185 (ZX)<br>0.2220 (ZY) |
| DGEDDS–Sand | 29.5140 (Reuss)<br>29.5247 (Voigt)<br>29.5194 (Hill) | 17.6058 (Reuss)<br>18.6088 (Voigt)<br>18.1073 (Hill) | 44.8274 (X)<br>45.7942 (Y)<br>50.9026 (Z) | 0.2807 (XY)<br>0.1971 (XZ)<br>0.2868 (YX) | 0.1967 (YZ)<br>0.2238 (ZX)<br>0.2186 (ZY) |
| AEOR–Sand | 29.4350 (Reuss)<br>29.4597 (Voigt)<br>29.4473 (Hill) | 17.7204 (Reuss)<br>18.7226 (Voigt)<br>18.2215 (Hill) | 45.1663 (X)<br>44.8343 (Y)<br>51.8890 (Z) | 0.2830 (XY)<br>0.1920 (XZ)<br>0.2809 (YX) | 0.1953 (YZ)<br>0.2206 (ZX)<br>0.2260 (ZY) |

The overall mechanical properties of DGEDDS after adsorption with sand were similar to those of DGEBA. However, the Young's modulus of DGEDDS displayed greater variation across different directions, and its Poisson's ratio also showed notable discrepancies among directions. This can be attributed to the presence of more polar groups within the DGEDDS molecule, which likely enhanced intermolecular forces and, consequently, its mechanical properties.

Conversely, the Young's modulus of AEOR after adsorption with sand varied considerably across different directions compared to the other two epoxy resins. It exhibited relatively lower shear modulus and bulk modulus values, suggesting weaker resistance to shear and volumetric deformation. Nevertheless, its Poisson's ratio was slightly higher in the ZY direction than those of the other epoxy resins, indicating increased susceptibility to transverse deformation in that direction.

The Poisson's ratios for the three epoxy–sand composites exhibit slight variations across different directions. The XY direction consistently displays the highest Poisson's ratio (approximately 0.28), while the YZ and XZ directions exhibit lower values (approximately 0.19–0.20). These discrepancies reflect the anisotropic deformation behavior of the sand under pressure.

Overall, the small differences in bulk modulus (29.5 $\pm$ 0.2 GPa) and shear modulus (18.1 $\pm$ 0.2 GPa) among the three epoxy resins implied a comparable resistance to volume deformation, likely due to their similar chemical structures and intermolecular forces.

### *3.4. Radius of Gyration Analysis*

A larger fluctuation in the radius of gyration indicates a greater degree of flexibility in the system, while a smaller fluctuation suggests a more rigid structure. The radius of

gyration of DGEBA, DGEDDS, and AEOR in their lowest energy conformations is shown in Figure 8. The Rg of all three polymer molecules increased compared to their initial states.

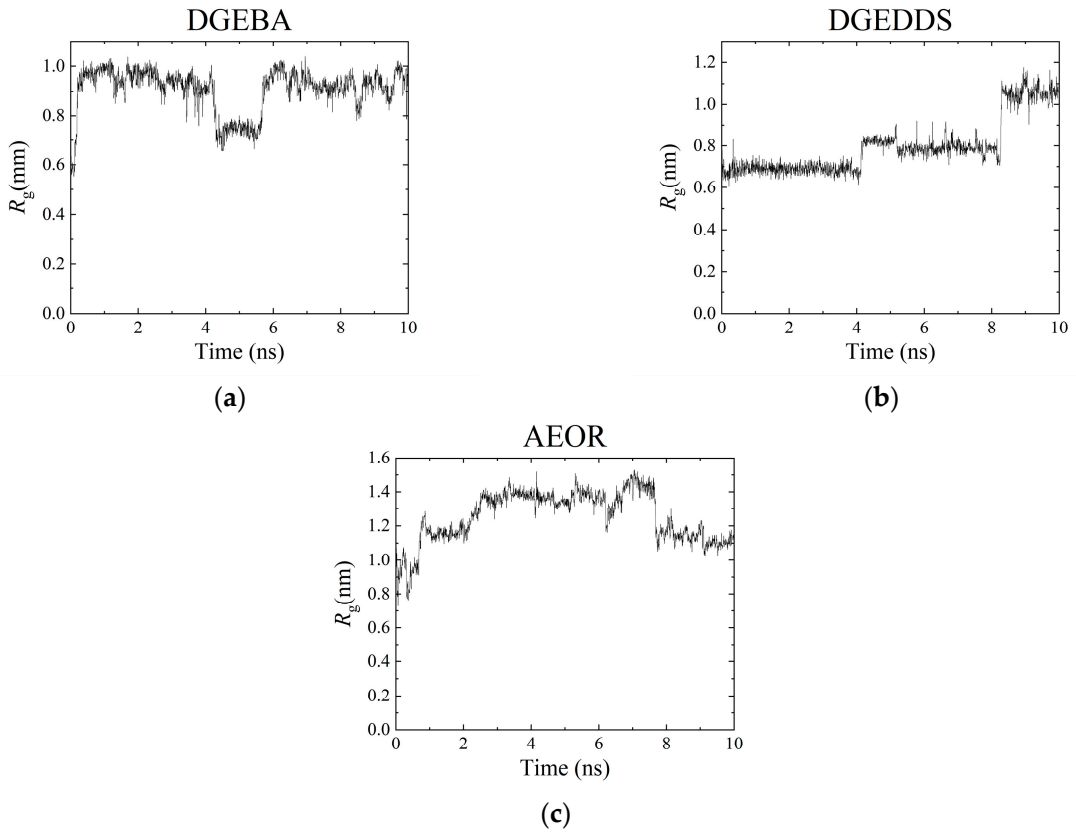


**Figure 8.** The radius of gyration of the three epoxy resins on the sand surface: (**a**) the radius of gyration of DGEBA–Sand; (**b**) the radius of gyration of DGEDDS–Sand; (**c**) the radius of gyration of AEOR–Sand.

For DGEBA, the Rg increased rapidly at the beginning and then stabilized, consistent with observations from its simulation trajectories. The DGEBA molecule was more compact and rigid than AEOR due to the presence of the bisphenol-A group. This rigidity was reflected in the smaller Rg value, averaging around 0.8–0.9 nm. The relatively stable Rg value in Figure 8a indicated that the molecule experiences less conformational change over the simulation time.

The DGEDDS molecule had a combination of rigid and flexible segments. The presence of the sulfur atoms within the molecule led to a greater conformational flexibility compared to that of DGEBA. The average Rg was between 0.8 and 1 nm. Figure 8b shows a more dynamic fluctuation of the Rg value for DGEDDS, suggesting a higher degree of conformational change compared to DGEBA.

The AEOR molecule had a relatively linear structure with long alkyl chains. This linearity contributed to a larger Rg value compared to the other two epoxy resins. Figure 8c shows a relatively constant value of around 1.1–1.2 nm. The high Rg of AEOR suggests that its structure was less compact, allowing for more flexibility and movement within the molecule.

The analysis of Rg values revealed distinct structural characteristics and flexibilities among the three epoxy resins (AEOR, DGEBA, and DGEDDS). AEOR, with its largest Rg, exhibited a more extended and flexible molecular conformation. In contrast, DGEBA, with a smaller and stable Rg, demonstrated a more compact and rigid structure. DGEDDS displayed an intermediate Rg value with significant fluctuations, indicating a mixed structure with both flexible and rigid segments. This dynamic nature of DGEDDS was evident in the

step-like Rg pattern observed within the first 10 ns of the simulation, where the molecule initially adsorbed to the surface with one end, then progressively stretched out and stabilized with the attachment of the other end. In contrast, the rigid structure of AEOR resulted in a stable Rg. The curve of DGEDDS exhibited a step-like pattern, with the Rg increasing twice within the first 10 ns of the simulation. Trajectory analysis revealed that one end of the oligomer chain initially attached to the sand surface. After a period of fluctuation, the other end also adsorbed to the sand surface, leading to a stretched molecular conformation on the sand surface, which then stabilized. AEOR, due to its rigid structure, exhibited a stable Rg, while DGEBA and DGEDDS, with their more flexible structures, displayed greater Rg fluctuations.

## 4. Conclusions

This study elucidated the curing mechanism of epoxy resins on sand by employing molecular dynamics simulations, encompassing DGEBA, DGEDDS, AEOR. The following conclusions were derived from the findings:

1. DGEDDS exhibited a significantly higher number of hydrogen bonds after adsorption, forming eight compared to zero for DGEBA and one for AEOR. This is because the high hydrogen bond density per unit molecular weight of DGEDDS after adsorption was $9.188 \times 10^{-3}$, which was larger than those obtained from DGEBA and AEOR. The results indicated that DGEDDS established stronger intermolecular interactions with sand compared to DGEBA and AEOR.
2. The mechanical properties of three epoxy resins (DGEBA, DGEDDS, and AEOR) after sand adsorption showed minimal significant differences. While DGEBA exhibited slightly higher shear and Young's moduli, approximately $18.1 \pm 0.2$ GPa and $29.5 \pm 0.2$ GPa, respectively, DGEDDS showed greater directional variability in these properties, potentially due to its increased polarity and enhanced intermolecular forces. AEOR, on the other hand, displayed the lowest shear and bulk moduli, indicating a weaker resistance to deformation.
3. DGEBA, with its more compact and rigid structure due to the bisphenol-A group, exhibited a smaller average Rg of 0.8–0.9 nm, while DGEDDS, containing sulfur atoms that increase flexibility, had a slightly larger average Rg of 0.8–1 nm. AEOR, characterized by its linear structure with long alkyl chains, displayed the largest Rg value, averaging 1.1–1.2 nm, indicating a more extended and flexible conformation. While DGEBA and DGEDDS displayed flexible conformations, AEOR maintained a notably rigid structure. These structural differences likely contributed to the varying mechanical properties observed for these epoxy resins after adsorption onto sand.

**Author Contributions:** D.S.: conceptualization, funding acquisition, supervision, writing—review and editing and validation; X.P.: writing—original draft, methodology, software, and validation; L.C.: project administration, funding acquisition, resources, and validation; X.W.: writing—review and editing, investigation, formal analysis, and validation; C.W.: visualization and data curation; R.L.: visualization and validation. All authors reviewed the manuscript. All authors have read and agreed to the published version of the manuscript.

**Funding:** The authors gratefully acknowledge the financial support of the Fundamental Research Funds for Central Universities of China (Grant No. B230201060) and JSTI Group (Grant No. 823088816).

**Institutional Review Board Statement:** Not applicable.

**Informed Consent Statement:** Not applicable.

**Data Availability Statement:** The raw data supporting the conclusions of this article will be made available by the authors on request.

**Conflicts of Interest:** Lili Cai and Chunying Wu were employed by the company Nanjing Ningtong Intelligent Transportation Technology Research Institute Co., Ltd. The remaining authors declare that the research was conducted in the absence of any commercial or financial relationships that could be construed as a potential conflict of interest.

## References


1. Lamb, V. Constructing the global sand crisis: Four reasons to interrogate crisis and scarcity in narrating extraction. *Extr. Ind. Soc.* **2023**, *15*, 101282. [CrossRef]
2. Smaida, A.; Haddadi, S.; Nechnech, A. Improvement of the mechanical performance of dune sand for using in flexible pavements. *Constr. Build. Mater.* **2019**, *208*, 464–471. [CrossRef]
3. Wang, P.; Yin, Z.Y. Micro-mechanical analysis of caisson foundation in sand using DEM. *Ocean Eng.* **2020**, *203*, 107240. [CrossRef]
4. Wang, K.; Miao, M.; Zhou, H. Effects of large-scale unloading on existing shield tunnels in sandy gravel strata. *Geotech. Geol. Eng.* **2021**, *39*, 3401–3416. [CrossRef]
5. Khare, G.; Kumar, V.; Sardana, S.; Vishwakarma, G.K. Geoenvironmental and geotechnical assessment of soil slopes in the vicinity of Atal tunnel in Himachal Pradesh, India. *Geomat. Nat. Hazards Risk* **2022**, *13*, 1251–1269. [CrossRef]
6. Barman, D.; Dash, S.K. Stabilization of expansive soils using chemical additives: A review. *J. Rock Mech. Geotech. Eng.* **2022**, *14*, 1319–1342. [CrossRef]
7. Consoli, N.C.; Daassi-Gli, C.A.P.; Ruver, C.A.; Lotero, A.; Scheuermann Filho, H.C.; Moncaleano, C.J.; Lourenço, D.E. Lime–ground glass–sodium hydroxide as an enhanced sustainable binder stabilizing silica sand. *J. Geotech. Geoenviron. Eng.* **2021**, *147*, 06021011. [CrossRef]
8. Baldovino, J.A.; de la Rosa, Y.E.N.; Calabokis, O.P. Insight on characterization through porosity-to-lime index of a stabilized soil for the long-term. *Case Stud. Constr. Mater.* **2024**, *20*, e02718. [CrossRef]
9. Onyelowe, K.C.; Moghal, A.A.B.; Ebid, A.; Rehman, A.U.; Hanandeh, S.; Priyan, V. Estimating the strength of soil stabilized with cement and lime at optimal compaction using ensemble-based multiple machine learning. *Sci. Rep.* **2024**, *14*, 15308. [CrossRef]
10. Nadeem, M.; Ullah, S.; Chen, S.; Alkahtani, M.Q.; Khan, M.A.; Salih, R.; Jian, L.; Mursaleen, M.; Islam, S.; Ahmad, J. Evaluation of engineering properties of clayey sand bio-mediated with terrazyme enzyme. *Front. Mater.* **2023**, *10*, 1195310. [CrossRef]
11. Raheem, B.S.; Oladiran, G.; Oke, D.; Musa, S. Evaluation of strength properties of subgrade materials stabilized with bio-enzyme. *Eur. J. Eng. Technol. Res.* **2020**, *5*, 607–610.
12. Vaddi, P.K.; Dey, S.; Bharath, C.N.; Pallavi, U. Effects of Bio-enzyme on the strength properties of soil. *Chem. Inorg. Mater.* **2024**, *3*, 100047.
13. Liu, J.; Chen, Z.; Kanungo, D.P.; Song, Z.; Bai, Y.; Wang, Y.; Li, D.; Qian, W. Topsoil reinforcement of sandy slope for preventing erosion using water-based polyurethane soil stabilizer. *Eng. Geol.* **2019**, *252*, 125–135. [CrossRef]
14. Park, S.S.; Lee, J.S.; Yoon, K.B.; Woo, S.W.; Lee, D.E. Application of an acrylic polymer and epoxy emulsion to red clay and sand. *Polymers* **2021**, *13*, 3410. [CrossRef] [PubMed]
15. Muguda, S.; Hughes, P.N.; Augarde, C.E.; Perlot, C.; Walter Bruno, A.; Gallipoli, D. Cross-linking of biopolymers for stabilizing earthen construction materials. *Build. Res. Inf.* **2022**, *50*, 502–514. [CrossRef]
16. Archibong, G.; Sunday, E.; Akudike, J.; Okeke, O.; Amadi, C. A review of the principles and methods of soil stabilization. *Int. J. Adv. Acad. Res. | Sci.* **2020**, *6*, 2488–9849.
17. Li, Y.; Fang, X.; Shen, C.; Jiang, W.; Huang, S.; Guoliang, M. Review of Bio-Enzyme for Soil Improvement. *Biogeotechnics* **2024**, 100143. [CrossRef]
18. Arabani, M.; Shalchian, M.M. A review of the use of bio-based substances in soil stabilization. *Environ. Dev. Sustain.* **2024**, *26*, 13685–13737. [CrossRef]
19. Chudzik, J.; Bieliński, D.M.; Demchuk, Y.; Bratychak, M.; Astakhova, O. Influence of Modified Epoxy Dian Resin on Properties of Nitrile-Butadiene Rubber (NBR). *Materials* **2022**, *15*, 2766. [CrossRef]
20. Gunka, V.; Hrynchuk, Y.; Prysiazhnyi, Y.; Demchuk, Y.; Sidun, I.; Reutskyy, V.; Bratychak, M. Investigation of the Impact of Epoxy Compounds Based on Environmentally Friendly and Renewable Raw Materials in Bitumen Modification Processes. In *Environmental Technology and Sustainability*; Apple Academic Press: Waretown, NJ, USA, 2024; pp. 97–126.
21. Liu, J.; Bai, Y.; Song, Z.; Kanungo, D.P.; Wang, Y.; Bu, F.; Chen, Z.; Shi, X. Stabilization of sand using different types of short fibers and organic polymer. *Constr. Build. Mater.* **2020**, *253*, 119164. [CrossRef]
22. Yuan, J.; Pei, Z.; Yang, S.; Yu, H.; Hu, X.; Liu, H. Preparation and characterization of an eco-friendly sand-fixing agent utilizing nanosilica/polymer composites. *J. Appl. Polym. Sci.* **2023**, *140*, e53804. [CrossRef]
23. Anastassiou, A.; Mavrantzas, V.G. Molecular structure and work of adhesion of poly(n-butyl acrylate) and poly(n-butyl acrylate-co-acrylic acid) on α-quartz, α-ferric oxide, and α-ferrite from detailed molecular dynamics simulations. *Macromolecules* **2015**, *48*, 8262–8284. [CrossRef]
24. Shi, Y.F.; Sun, Y.Y.; Gao, B.; Xu, H.X.; Wu, J.C. Importance of Organic Matter to the Retention and Transport of Bisphenol A and Bisphenol S in Saturated Soils. *Water Air Soil Pollut.* **2019**, *230*. [CrossRef]
25. Jiang, T.W.; Reddy, K.S.K.; Chen, Y.C.; Wang, M.W.; Chang, H.C.; Abu-Omar, M.M.; Lin, C.H. Recycling Waste Polycarbonate to Bisphenol A-Based Oligoesters as Epoxy-Curing Agents, and Degrading Epoxy Thermosets and Carbon Fiber Composites into Useful Chemicals. *ACS Sustain. Chem. Eng.* **2022**, *10*, 2429–2440. [CrossRef]
26. Zhu, J.; Shen, D.J.; Jin, B.S.; Wu, S.X. Theoretical investigation on the formation mechanism of carbonate ion in microbial self-healing concrete: Combined QC calculation and MD simulation. *Constr. Build. Mater.* **2022**, *342*, 128000. [CrossRef]
27. Zhu, J.; Shen, D.J.; Wu, W.; Jin, B.S.; Wu, S.X. Hydration inhibition mechanism of gypsum on tricalcium aluminate from ReaxFF molecular dynamics simulation and quantum chemical calculation. *Mol. Simul.* **2021**, *47*, 1465–1476. [CrossRef]

28. Zhu, J.; Shen, D.J.; Xie, J.J.; Jin, B.S.; Wu, S.X. Transformation mechanism of carbamic acid elimination and hydrolysis reaction in microbial self-healing concrete. *Mol. Simul.* **2022**, *48*, 719–735. [CrossRef]
29. Zhu, J.; Shen, D.J.; Xie, J.J.; Tang, C.M.; Jin, B.S.; Wu, S.X. Mechanism of urea decomposition catalyzed by Sporosarcina pasteurii urease based on quantum chemical calculations. *Mol. Simul.* **2021**, *47*, 1335–1348. [CrossRef]
30. Wang, H.; Zhang, H.; Liu, C.B.; Yuan, S.L. Coarse-grained molecular dynamics simulation of self-assembly of polyacrylamide and sodium dodecylsulfate in aqueous solution. *J. Colloid Interface Sci.* **2012**, *386*, 205–211. [CrossRef]
31. Prasitnok, O.; Prasitnok, K. Molecular dynamics simulations of copolymer compatibilizers for polylactide/poly (butylene succinate) blends. *Phys. Chem. Chem. Phys.* **2023**, *25*, 5619–5626. [CrossRef]
32. Ma, S.J.; Chen, P.; Xu, J.L.; Xiong, X.H. Molecular dynamics simulations of key physical properties and microstructure of epoxy resin cured with different curing agents. *J. Mater. Sci.* **2022**, *57*, 1123–1133. [CrossRef]
33. Huang, W.; Geng, X.Y.; Li, J.; Zhou, C.Y.; Liu, Z. Molecular dynamics study on the adsorption and modification mechanism of polymeric sand-fixing agent. *Polymers* **2022**, *14*, 3365. [CrossRef] [PubMed]
34. Liu, J.; Shi, B.; Jiang, H.T.; Huang, H.; Wang, G.H.; Kamai, T. Research on the stabilization treatment of clay slope topsoil by organic polymer soil stabilizer. *Eng. Geol.* **2011**, *117*, 114–120. [CrossRef]
35. Lyu, W.; Zhou, Z.; Huang, J.; Yan, K. Study on adsorption behavior of a new type gemini surfactant onto quartz surface by a molecular dynamics method. *Nano* **2022**, *17*, 2150151. [CrossRef]
36. Quezada, G.R.; Piceros, E.; Saavedra, J.H.; Robles, P.; Jeldres, R.I. Polymer affinity with quartz (101) surface in saline solutions: A molecular dynamics study. *Miner. Eng.* **2022**, *186*, 107750. [CrossRef]
37. Cheng, Z.Y.Y.; Zhu, Y.M.; Li, Y.J.; Butt, S. Experimental and MD simulation of 3-dodecyloxypropanamine and 3-tetradecyloxypropylamine adsorbed onto quartz (1 0 1) surface. *Int. J. Min. Sci. Technol.* **2021**, *31*, 1033–1042. [CrossRef]
38. Zhang, B.Q.; Yang, X.B.; Sun, Z.Q.; Miao, Z.J.; Wang, H.D.; Lyu, Y. Modification treatment and properties research of fiber reinforced silicon dioxide composites. *Cailiao Gongcheng/J. Mater. Eng.* **2020**, *48*, 48–53. [CrossRef]
39. Zhang, J.J.; Li, B.; Yu, C.; Zhang, M.Y. Mechanical properties of slag-fly ash based geopolymer stabilized sandy soil. *Yantu Lixue/Rock Soil Mech.* **2022**, *43*, 2421–2430. [CrossRef]
40. Lim, S.J.; Kim, D.S. Effect of functionality and content of epoxidized soybean oil on the physical properties of a modified diglycidyl ether of bisphenol A resin system. *J. Appl. Polym. Sci.* **2021**, *138*, 50441. [CrossRef]
41. Dagdag, O.; Harfi, A.E.; Essamri, A.; Bachiri, A.E.; Hajjaji, N.; Erramli, H.; Hamed, O.; Jodeh, S. Anticorrosive performance of new epoxy-amine coatings based on zinc phosphate tetrahydrate as a nontoxic pigment for carbon steel in NaCl medium. *Arab. J. Sci. Eng.* **2018**, *43*, 5977–5987. [CrossRef]
42. Varganici, C.D.; Rosu, L.; Rosu, D.; Hamciuc, C.; Rosca, I.; Vasiliu, A.L. Effect of hardener type on the photochemical and antifungal performance of epoxy and oligophosphonate S–IPNs. *Polymers* **2022**, *14*, 3784. [CrossRef] [PubMed]
43. Xu, D.; He, Y.; Liu, X.; Xiong, C.; Zhou, X.; Xue, C.; Ji, H. N-Hydroxyphthalimide-Catalyzed Epoxidation of Inactive Aliphatic Olefins with Air at Room Temperature. *Asian J. Org. Chem.* **2021**, *10*, 3349–3354. [CrossRef]
44. Ruehlmann, J.; Korschens, M. Soil particle density as affected by soil texture and soil organic matter: 2. Predicting the effect of the mineral composition of particle-size fractions. *Geoderma* **2020**, *375*, 114543. [CrossRef]
45. Chuang, I.S.; Maciel, G.E. Probing hydrogen bonding and the local environment of silanols on silica surfaces via nuclear spin cross polarization dynamics. *J. Am. Chem. Soc.* **1996**, *118*, 401. [CrossRef]
46. Bone, M.A.; Macquart, T.; Hamerton, I.; Howlin, B.J. A novel approach to atomistic molecular dynamics simulation of phenolic resins using symthons. *Polymers* **2020**, *12*, 926. [CrossRef]
47. Meunier, M.; Robertson, S. Materials studio 20th anniversary. *Mol. Simul.* **2021**, *47*, 537–539. [CrossRef]
48. Sun, H. COMPASS: An ab initio force-field optimized for condensed-phase applications overview with details on alkane and benzene compounds. *J. Phys. Chem. B* **1998**, *102*, 7338–7364. [CrossRef]
49. Schneider, H.-J. Noncovalent interactions: A brief account of a long history. *J. Phys. Org. Chem.* **2022**, *35*. [CrossRef]
50. Zuo, X.; Wang, B.; Ejeromedoghene, O.; Ye, S.; Fu, G. Performance exploration of polyvinyl alcohol/modified glass fiber composites based on hydrogen bonding interactions. *J. Mol. Struct.* **2023**, *1294*. [CrossRef]
51. Yan, L.J.; Yang, Y.; Jiang, H.; Zhang, B.J.; Zhang, H. The adsorption of methyl methacrylate and vinyl acetate polymers on α-quartz surface: A molecular dynamics study. *Chem. Phys. Lett.* **2016**, *643*, 1–5. [CrossRef]
52. Tavakoli, D.; Tarighat, A. Molecular dynamics study on the mechanical properties of Portland cement clinker phases. *Comput. Mater. Sci.* **2016**, *119*, 65–73. [CrossRef]
53. Hill, R. The elastic behaviour of a crystalline aggregate. *Proc. Phys. Soc. Sect. A* **1952**, *65*, 349. [CrossRef]